Quantitative deconvolution microscopy

10

Paul C. Goodwin[*,†]
GE Healthcare, Issaquah, Washington, USA
†*Department of Comparative Medicine, University of Washington, Seattle, Washington, USA*

CHAPTER OUTLINE

Abstract

The light microscope is an essential tool for the study of cells, organelles, biomolecules, and subcellular dynamics. A paradox exists in microscopy whereby the higher the needed lateral resolution, the more the image is degraded by out-of-focus information. This creates a significant need to generate axial contrast whenever high lateral resolution is required. One strategy for generating contrast is to measure or model the optical properties of the microscope and to use that model to algorithmically reverse some of the consequences of high-resolution imaging. Deconvolution microscopy implements model-based methods to enable the full diffraction-limited resolution of the microscope to be exploited even in complex and living specimens.

INTRODUCTION

Microscopes are some of the most ubiquitous tools in the biological laboratory, yet most scientists use them without knowing much about them or the fundamental physics necessary to get the most from them. Our look at quantitative deconvolution microscopy will begin with a look at the microscope itself. In order for a microscope to be useful, it must fulfill three functions: magnification, resolution, and contrast. A microscope that delivers one or two of these attributes but not all three is of little value. We start by looking at each of these attributes and how they affect the image from the microscope. The process of looking at these attributes elucidates the limitations of the microscope and motivates this chapter.

Magnification, for the sake of this chapter, will be defined as the portion of the field of view that is projected onto the detector. Compared to the field of view of a human eye, five times ($5\times$) magnification would project one-fifth of the lateral dimensions onto the eye. Since magnification takes place in both lateral dimensions, the area reduction is the magnification squared or 1/25 in the case of the $5\times$ objective. The general formula is

$$\mathrm{FOV} = \frac{1}{M^2} \tag{10.1}$$

This has a profound effect on the amount of signal that can be collected with increasing magnification. For a fixed light collection efficiency (to be discussed later), the amount of signal from a sample also falls according to this relationship:

$$\mathrm{Brightness} = \frac{1}{M^2} \tag{10.2}$$

If we start with a given field of view that generates a total of one million photons per second and view that area with a $5\times$ objective, the number of photons drops to 40,000. For a $100\times$ objective, the number of photons drops to only 100 photons. This has a significant impact on the contrast of the image. The statistical noise (Poisson noise) in the image is

$$\mathrm{Noise_{Poisson}} = \sqrt{\mathrm{Events}} \tag{10.3}$$

The consequences of magnification on the signal-to-noise ratio (SNR) can be seen in Table 10.1.

Table 10.1 Effect of increased magnification on SNR

Magnification	Photons	Noise	SNR
$1\times$	1,000,000	1000	1000:1
$5\times$	40,000	200	200:1
$100\times$	100	10	10:1

The SNR drops from 1000:1 to 10:1 purely as a consequence of the magnification change from $1\times$ to $100\times$. So, how do we overcome this loss? The answer is in the numerical aperture (NA) of the objective lens. NA is defined as

$$NA = n * \sin(\Theta) \tag{10.4}$$

where n is the lowest index of refraction between the sample and the front of the objective lens and theta (Θ) is the half angle that describes the cone of light that can be effectively captured by a given lens. The consequence of a larger cone (higher NA) is that many more photons can be collected. Overall, the relative brightness is proportional to the NA to the fourth power divided by the magnification squared:

$$\text{Brightness} \propto \frac{NA^4}{M^2} \tag{10.5}$$

Some examples of brightness for known lenses are given in Table 10.2.

As you can see, the loss of brightness as a consequence of magnification is more than compensated for by a concomitant increase in NA. On the surface, this is beneficial because the resolution also increases with NA. In fact, Z resolution increases with NA^2 so this would seem to be advantageous for microscopy. The problem is demonstrated in Fig. 10.1.

Table 10.2 Relative brightness of common objective lenses

Magnification	NA	FOV	Brightness
1	0.157	1.00000	1.000
5	0.15	0.04000	0.033
10	0.40	0.01000	0.421
20	0.85	0.00250	2.148
40	1.30	0.00063	2.938
60	1.42	0.00028	1.859
100	1.40	0.00010	0.632
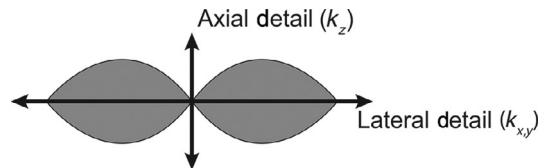
FIGURE 10.1

Lateral and axial contrast as a function of spatial detail. Lateral ($k_{x,y}$) and axial (k_z) contrast as a function of spatial detail in a microscope. Notice that the lateral detail (resolution) is well supported by significant contrast, while the axial detail is poorly supported; consequently, with increasing NA, a thinner image plane is in focus, while the out-of-focus contribution from adjacent planes is still present. The overall effect is higher axial blur in images as a function of higher NA.

As you can see, while the resolution along the Z-axis increases, there is no gain in the axial contrast with NA. In other words, as NA increases, the contribution of blurred (out-of-focus) information actually increases. So, the dimmer and smaller something is, the more problem there is with blur in the image. This is referred to as "the missing cone," and it has led microscopists to seek ways of generating axial contrast in order to be able to increase the sensitivity and in-focus information. Some of those methods include mechanical sectioning, deconvolution microscopy, confocal microscopy, multiphoton microscopy, and selective plane illumination. This chapter focuses on deconvolution microscopy. With the exception of mechanical sectioning, all of these methods are reserved for fluorescence and do not apply to transmissive imaging. In a transmissive image such as the absorption of light by a chromogen or stain, the intensity at each point is the sum of the absorptions along a ray from the light source to the sample. While the absorption of light along that ray is linearly related to mass (per Beer's law), the exact location of each chromogen is difficult to assess. In fluorescence, the measured light originates at the fluorochrome. This greatly simplifies the mathematical model of the microscope and enables advanced optical methods such as confocal microscopy.

10.1 THE POINT-SPREAD FUNCTION

The resolution of the microscope is finite. In fluorescence microscopy (where the condenser and the objective lens are the same lens), the resolution (D) is given as

$$D = \frac{0.61 * \lambda}{\text{NA}} \text{(Rayleigh criterion)} \tag{10.6}$$

So, for green fluorescence emitted from eGFP (em $=510$ nm) and an ideal 1.4 NA objective, the resolution could be as good as 222 nm (per Rayleigh). The consequence is that any object that is smaller than 222 nm will project to a minimum of 222 nm. But it is actually more complicated in three dimensions. If one were to measure how a single point of light spreads through space, he or she would visually describe the blurring that occurs in the microscope. Such a measurement is called the point-spread function (PSF).

One can view the PSF by collecting a set of images of a fluorescent bead sitting on a cover glass. Starting away from the plane of best focus, one can collect a series of images approaching the plane of best focus and moving beyond that plane of focus. Figure 10.2 shows two views of the image series. Panel (A) shows a through-focus series of the PSF enhanced to show the low intensity values by expressing the displayed intensities as the third power of the actual values, that is, $D = I^3$. Panel (B) shows the image series as an orthogonal view through the same PSF.

As you can see in panel (A), the out-of-focus bead generates a series of rings that narrow as they become the closer to the optimum focus and that then spread out again in a symmetrical fashion as the focus is passed. The symmetry of the spread of the rings laterally and through the focus is indicative of the optical conditions and the
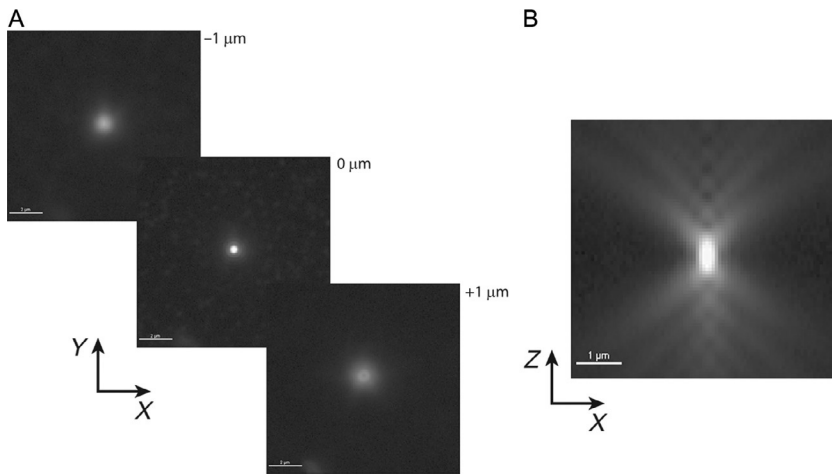
FIGURE 10.2

Lateral and axial views of the point-spread function (PSF). The point-spread function (PSF) of a good-quality lens is marked by lateral and axial symmetry. Panel (A) shows how the PSF of a good lens is symmetrical about the center of the image as the microscope is focused one micrometer below (-1 μm), in the middle of (0 μm), and 1 μm above ($+1$ μm) the plane of best focus. Panel (B) is a representation of an X–Z section through the same bead in panel (A). To generate the X–Z section, a series of X–Y images were collected at 0.2 μm spacing through the focus of a single fluorescent latex bead (0.1 μm diameter). A software is then used to properly scale and orthogonally section the stack of X–Y images into the single X–Z section presented. For both panels, the intensities are displayed and raised to the third power (display $= I^3$) as discussed in the text.

quality of the objective lens and can be used to evaluate optical systems (Goodwin, 2007). Even in the best case, these images are not simple to collect and interpret and in the case of optical aberrations become quite complex. Importantly, the PSF demonstrates how each point source of light in the object is spread. So, any image acquired in the microscope is actually the summation of all of the overlapping PSFs from each subresolution point in space. This is expressed as the imaging formula

$$I_{Image} = I_{Actual} \otimes PSF \tag{10.7}$$

The frustration of every microscopist is that they never see the actual object (I_{Actual}). All they can ever see is a projection of the object blurred by the PSF (I_{Image}). This is illustrated in Fig. 10.3.

The term convolution ($\otimes$) is a specific mathematical description of the physical phenomenon of the overlap of the PSFs. One analogy is that of a paint brush that dabs a pattern (the PSF) on every point in the object. Deconvolution is a mathematical process that seeks to reverse this process and restore an image that more closely approximates the image of the original object.
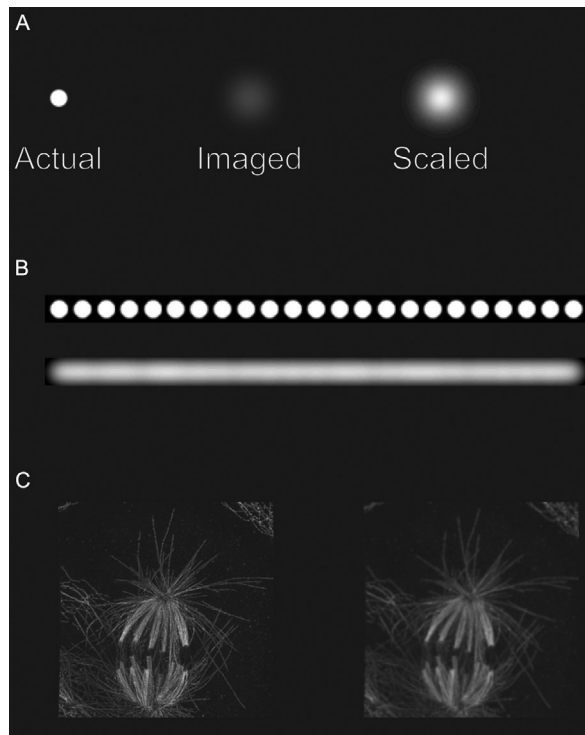
FIGURE 10.3

The effect of inherent blur in microscopy. Since the NA of the objective lens is limited, complete knowledge of the actual object is not obtained in the light microscope (see Eq. 10.7). The image that is obtained (I_{Image}) is the actual object (I_{Actual}) convolved with the PSF. Panel (A) shows the effect of this blurring on a single point of fluorescence. The actual object is blurred resulting in a spreading and reduction of the intensity of the object (Imaged). If the image is scaled (Scaled), one can see the significant spreading that occurs. If one were to then take a series of points in a row (panel B) and blur those, they would appear as a continuous line. The effect that this has on real object, in this case a PTK1 cell labeled with a fluorescent antibody against b-tubulin, is evident in panel (C, right). While considerably more detail can be seen in a superresolution image of the cell (panel C, left), the resolution of the object is substantially decreased when imaged with diffraction-limited optics.

Fluorescent sample kindly provided by Dr. Keith DeLuca, University of Colorado.

10.2 DECONVOLUTION MICROSCOPY

Deconvolution microscopy is an image-processing method that seeks to computationally reverse the effects of the blurring in the microscope. There are generally two types of deconvolution: deblurring and image restoration.

10.2.1 **DEBLURRING**

Deblurring (also called nearest-neighbor deconvolution, multineighbor deconvolution, etc.) is a fast algorithm for reducing blur in an image. It has the advantage that it is quickly calculated but has the disadvantage that it tends to be noisy and that the results produced are not generally linear (Fig. 10.4):

$$\text{Deconvolved}\left(n_j\right) = n_j - \left(n_{j-1} \otimes \text{PSF}_{\text{Est}}\right) - \left(n_{j+1} \otimes \text{PSF}_{\text{Est}}\right) \tag{10.8}$$

The image taken in a given focal plane is the object at that plane blurred by the in-focus PSF and the out-of-focus contribution from the objects above and below that plane. Deblurring attempts to estimate the contribution attributable to the out-of-focus image planes and subtract them from the in-focus image plane. To estimate the contribution of the out-of-focus planes, the images taken at the adjacent image planes $n(j-1)$ and $n(j+1)$ are each blurred by an estimate of the PSF (based on NA). In multineighbor deblurring, the contribution for further adjacent planes such as $n(j-2)$ and $n(j-2)$ is also blurred and subtracted from the image plane. As mentioned, these calculations are fast but they are prone to two problems. First, since it is a subtractive process, the SNR of the resulting image is reduced. The signal is lost from subtraction and the noise is increased by the propagation of error. Second, the intensity of a given location is significantly influenced by the imprecision in the estimation of the contribution of out-of-focus objects, such that linearity is lost. The contribution from neighboring objects can only be estimated since their intensity is also not known (along with the in-focus object). The estimation of blurring the out-of-focus planes before subtraction does not adequately describe their contribution. As a consequence, deblurring should never be used when intensity is intended to represent actual mass of fluorochromes in a location.

Deblurring becomes less relevant as computational power increases. In the 1990s, when these methods were made popular, the computational power necessary for proper image restoration was too expensive. Advances in computational speed have rendered these deblurring algorithms as unnecessary, but they still persist in some software applications.
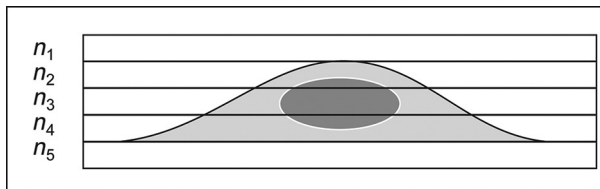
FIGURE 10.4

Nearest-neighbor deconvolution. In this figure, a cell is imaged by taking five images (n_1, n_2, n_3, n_4, and n_5) at successive focal planes through the object. The images in adjacent images can be used to subtract their contribution. See text for details.

10.2.2 **IMAGE RESTORATION**

Image restoration turns back to the imaging equation in Eq. (10.7). By making a careful measure of I_{Image} and the PSF, one can use mathematics to derive the best estimate of the actual object (I_{Object}) that when blurred by the PSF generates the measured I_{Image}. But how is this accomplished?

10.2.3 **FOURIER TRANSFORMS**

Jean Baptiste Joseph Fourier (1768–1830) was a French polymath. Among many of his activities, he was attempting to model how heat transfers through metals. This ended up being critical to making improvements to the steam engine that had been introduced earlier by James Watt. As Fourier worked on the model, he realized that he had insufficient mathematical tools to solve the problem, so he created new tools. These tools were built around his realization that any waveform could be expressed in terms of a series of cosine waves with different amplitudes and phase (now referred to as a Fourier series). By converting complex waveforms into a Fourier series, certain types of functions that were very difficult or impossible to solve without the tool became solvable. The complex form could be converted into frequency space (cosine functions with different amplitudes and phases), simple algebra could be used to solve the equations, and the results could be converted back into real space to provide the solution. The process is analogous to using logarithms to solve complex multiplications, convert the numbers to logs, add the numbers, and then convert the results back into decimal values. For a thorough description of Fourier methods, the reader is referred to Goodman (2005).

In the case of image restoration as described in the preceding text, we need to work around the term "blurred with the PSF." In real space, this is a very difficult concept, and it is mathematically difficult to solve for this notion of blurring with the PSF. The process is called convolution (symbolized as $\otimes$) and it is a bit complex to solve for 3D space. In the frequency space, convolution simply becomes multiplication. Taking the imaging formula (Eq. 10.7), we can transform it to frequency space as

$$F'\left(I_{\mathrm{Image}}\right) = F'(I_{\mathrm{Actual}}) \times F'(\mathrm{PSF}) \tag{10.9}$$

where F' represents the Fourier transform. The terms of the equation can be rearranged to

$$F'(I_{\mathrm{Actual}}) = \frac{F'\left(I_{\mathrm{Image}}\right)}{F'(\mathrm{PSF})} \tag{10.10}$$

By now taking the reverse Fourier transform of this ratio, we can now solve for the I_{Actual}. This method is referred to as the inversion solution. While relatively simple, the problem with this method is noise. Whenever a measurement is made, there is uncertainty. At the limit of resolution for the I_{Image} and the PSF, the values approach zero and the noise dominates the measures, resulting in significant errors

caused by dividing by zero. To avoid these problems, more elegant solutions are normally deployed. While space limitations preclude an exhaustive review of all published methods, the following sections describe a few of the more common methods.

10.2.4 ITERATIVE METHODS

Iteration is a method of solving equations that overcomes the problems of dividing by values close to zero. In the case of image restoration, the steps are as follows:

1. I_{Actual} is estimated (I_{Estimate}).
2. I_{Estimate} is then blurred with the PSF (I_{Blur}).
3. I_{Blur} is compared to I_{Image} resulting in I_{Residual}.
4. Refine I_{Estimate} based on I_{Residual}.
5. Repeat 2–4 minimizing I_{Residual}.

This represents the simplest form of iterative deconvolution algorithm. In practice, as was discussed in the preceding text, every measurement contains noise. This noise leads to instabilities in this simplest form. A number of modifications have been made to this simplest form to incorporate a priori constraints. These constraints stabilize the algorithm, reduce the number of iterations necessary to obtain an acceptable outcome, and can somewhat extend the resolution of the image (Mertz, 2010). One form of constraint is to limit the noise by periodically introducing a smoothing operation, such that I_{Estimate} is periodically blurred. Another form of constraint sets any negative values to zero when updating I_{Estimate}, based on the observation that negative intensity is non-sensical (Goodman, 2005; Mertz, 2010; Wallace, Schaefer, & Swedlow, 2001). This method was first introduced by Gold and refined by Agard (Agard, 1984; Gold, 1964; Swedlow et al., 1997) based on modifications to the original methods of Jansson (Jansson, 1997) and Van Cittert (Frieden, 1975). The treatment of noise is generally referred to as "noise regularization." A full treatment of these methods is beyond the reach of this chapter, and the user is instead referred to Wallace et al. (2001), Mertz (2010), Conchello (1998), Holmes (1992), McNally, Karpova, Cooper, and Conchello (1999), Shaw (1993), and Shaw and Rawlins (1991).

   In some cases, the PSF is not known. Estimating the PSF through first principles (Goodman, 2005, Shaw, 1993, Shaw & Rawlins, 1991) can be used, but in our experience, these methods do not fully account for the resolution empirically observed (Hiraoka, Sedat, & Agard, 1990). In addition, in some samples, the PSF is highly variable throughout the volume of the sample. To overcome these limitations, a class of algorithms have been developed that solve for both the object (I_{Actual}) and the PSF. This class of algorithms are referred to as "blind deconvolution" (Holmes, 1992) and in some cases have proved to be quite effective, especially when the performance of the entire optical system (including the sample) is difficult to assess. For an approachable discussion of these and other methods, the reader is referred to Wallace et al. (2001).

10.2.5 THE IMPORTANCE OF IMAGE QUALITY

The age-old axiom of "garbage in, garbage out" certainly applies to all image-processing methods and deconvolution in particular. Like many methods, deconvolution microscopy assumes a model for the microscope and optics and uses that model to extract more information from the data. The degree to which the actual microscope matches the model used will determine the quality of the restored image. If the microscope is well matched to the model, then the restored image will closely approximate the actual object. If the microscope is poorly matched to the model, then the restored image will have little in common with the actual object. In the latter case, the model needs to be adapted to accommodate the unexpected behavior. For poorly behaved systems, these adaptations will adversely affect the quality and quantitative nature of the restored images.

10.2.5.1 Factors that affect image restoration

1. Geometry—As we have explored earlier, restorations generally rely on 3D data sets. The microscope model assumes that the geometry of the data accurately reflects the geometry of sample. For example, many algorithms perform the deconvolution in spatial coordinates and not pixel coordinates. This is a more precise way of estimating the object but it requires that the pixel geometry is known. Importantly, it requires that the Z-step size is precise (consistent) and uncoupled to the X-axis and Y-axis. If the Z-step size is variable, then the geometry of the data does not match the geometry of the sample, and deconvolution will struggle. Likewise, a common problem in microscope stages is cross coupling of the axes. In cross coupling, movements in one axis, say Z, induce changes in an orthogonal axis (X and/or Y). This results in misalignment of the image data and poor agreement between the sample and the data.

2. Intensity—Image restoration assumes that differences in pixel intensities reflect differences in the mass of material at each position in space. If the relationship between mass and intensity is variable, then the restoration will poorly reflect the sample. Factors that affect the mass–intensity relationship include variable illumination, photobleaching, and nonlinear fluorescence. The intensity of a given volume pixel (voxel) is a function of the input light (illumination), the detection efficiency, and the mass of available fluorescent molecules. Changes in each of these parameters will affect the mass–intensity relationship. Illumination intensity at each point in the sample starts with spatial and temporal stability of the light source (Chapter 1). Light uniformity can be maximized by assuring that the microscope is properly aligned for Koehler illumination. Temporal fluctuations in lamp intensity can be normalized using the integrated intensity of each Z-plane. Since there is little expected change in integrated intensity between planes with wide-field microscopy and Koehler illumination, then this model can be effective. With other illumination schemes, these methods may or may not work. Illumination stability is also affected by debris and defects in the light path including the excitation filter and dichromatic

beam splitter. These should be clean and free of these defects (Chapter 4). Likewise, changes in detection efficiency (emission filter defects, camera gain noise, etc.) can also affect how well the restored image reflects the sample. Finally, there are changes in fluorochrome that can affect the model. If the mass of available fluorochrome changes through the experiment (e.g., photobleaching), then the intensity–mass relationship is perturbed. Also, changes in quantum yield due to fluorochrome saturation, quenching, and the local environment (solvent effects) can all lead to artifacts that will affect the appropriateness of the model and thus the quality of the deconvolution process. Some of these can be mitigated by experimental condition (choice of fluorochrome, illumination intensity, etc.) or corrected using a suitable model (photobleaching), but the user should be aware of the limitations of this or any other method.

3. Optics—The best resolution that an optical system can achieve is when the system is free of aberrations. Any deviations from the ideal can only degrade the resolution and contrast in the system. Optical aberrations can be caused by defects in the microscope itself (objective lenses, tube lens, etc.), and the microscope should be tested for these defects (Goodwin, 2007). However, most users are unaware of the effects of the sample on optical quality. Even if the microscope is free of defects and aberrations, the optical properties between the specimen and the front lens of the objective significantly contribute to the overall optical system. Some of these defects are difficult to avoid, for example, imaging through a cell wall (in plants and some microbes), a cuticle (such as a drosophila embryo), or high-refractive-index surfaces (like neural tissue). However, in many cases, the sample effects are avoidable. For example, dirt and smudges on the cover glass, mixing different immersion oils, improper mounting of the media, tilted cover glass, and uncorrected spherical aberration all significantly degrade the reconstruction because they are not included in the model. While one could construct a much more complex imaging model, it is more generally applicable to fix the problems that can be fixed (the smudges and such) and reserve improvements in the model for those attributes that are not easily fixed (e.g., the diffraction limit).

10.3 RESULTS

One way to assess the effects of deconvolution is to visually inspect the outcome, but this is a qualitative measure that lacks exactness. Another way is to take the Fourier spectrum of images pre- and postdeconvolution. In the case of Fig. 10.5B and D, the spectrum represents the Fourier spectrum of the images pre- and postdeconvolution (A and C, respectively). In this representation, the Fourier spectrum is plotted such that the low-frequency components (those values that are spatially variant over large distances) are plotted toward the center. As one expands radially from the center, higher-frequency components (the intensity fluctuations that are spatially variant
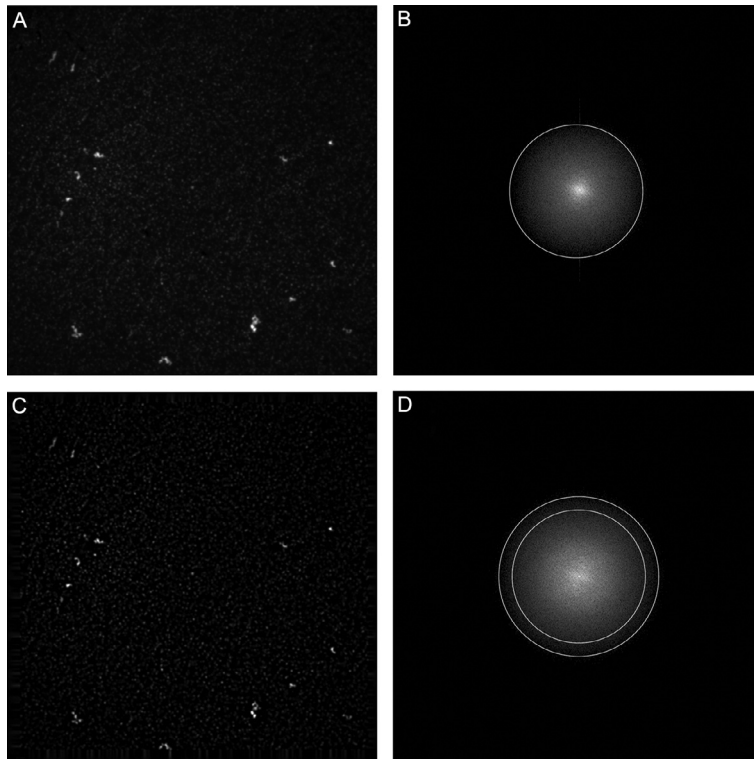
FIGURE 10.5

Resolution enhancement with deconvolution. Panel (A) represents the image of a single field of view of fluorescently labeled 0.10-µm beads dried onto a coverslip. Panel (B) represents the Fourier spectrum of the image in panel (A) scaled to illustrate the weak values in the image. In this representation of the Fourier spectrum, the contrast of low spatial detail is plotted in the center of the image and spatial detail increases toward the perimeter. The white circle illustrates the spatial frequency at which the contrast falls to background levels. Panel (C) represents the data in panel (A) after deconvolution was applied, and similarly, panel (D) represents the Fourier spectrum of that image. The outer circle illustrates the resolution limits after deconvolution as compared with the resolution limit prior to deconvolution (inner circle). See text for details.

over short distances) are plotted. The intensity of the Fourier spectrum (in this case squared) represents the contrast observed at that particular spatial frequency. The extent to which the spectrum spreads laterally is a measure of the lateral resolution. This spectrum also extends axially but is not displayed here. If the Fourier spectrum of one image extends further radially than another, it indicates that the spatial frequencies are higher than those in the other image.

In the case of Fig. 10.5B and D, the circles are approximations of the extent of the Fourier spectrum and are presented merely for clarity. In panel (D), the inner circle

represents the extent of the spectrum in the image predeconvolution. The outer circle represents the extent of the spectrum postdeconvolution. As can be seen, in this example, the deconvolution process extended the resolution approximately 20%. In reality, the resolution improvement is even less. Most of the apparent improvement is the result of an increase in contrast (signal-to-background) due to deconvolution. All of the resolution in the postdeconvolution image (panel C) was present in the predeconvolved image (panel A); however, the resolution was not accessible due to a lack of contrast. In the predeconvolution image, blur throughout the volume of the image increases the background of the image. After deconvolution, the background intensities contributed by blur are assigned to their proper locations in space, resulting in not only a decrease in background but also a substantial increase in integrated intensities in the objects. This contrast (signal-to-background) improvement ranges from 10- to 100-fold depending on the extent of out-of-focus objects.

10.3.1 ASSESSING LINEARITY

The wide-field fluorescence microscope is generally considered to be a linear instrument. That is, over the majority of the dynamic range of the instrument, there exists a linear relationship between the mass of fluorochrome in the original sample and the observed fluorescence intensity. This is especially true for instruments that conform to the ideal model of the microscope discussed in the preceding text. This linearity allows for intensity measurements to be made and compared and for these comparisons to be correlated to mass changes in the actual object. Is this linearity maintained with deconvolution? Does the integrated intensity of an object postdeconvolution bear a mass relationship with fluorochrome in the actual objects? In short, it depends. Some systems and methods maintain the mass relationship, while others do not. No comprehensive assessment of the linearity of all imaging systems exists but one method of assessing linearity was published (Swedlow, Hu, Andrews, Roos, & Murray, 2002; Swedlow, 2007). In their method, Swedlow et al. obtained 2.5-μm latex beads with six different relative concentrations of fluorochrome over 3.5 orders of magnitude. The intensities of the beads were measured using fluorescence-activated cell sorting (FACS) including the means and coefficients of variation. Beads were then mixed and dried onto coverslips, and image stacks were collected with a wide-field microscope. The volumetric integrated intensity of the beads with pre- and postdeconvolution was compared to the distributions measured by FACS with comparable results over three orders of magnitude. The weakest intensity beads were shifted in mean and coefficient of variability. It should be noted that, in this paper and the test samples used, both wide-field and deconvolution methods fared better than confocal systems. In the presence of optical aberrations, such as spherical aberration, the confocal system would be expected to fair even worse (White, Errington, Fricker, & Wood, 1995). For this study, Swedlow et al. used the Agard constrained iterative method mentioned previously.

10.3.2 **APPLICATIONS OF DECONVOLUTION MICROSCOPY**

The contrast and resolution improvements afforded by deconvolution microscopy can be exceptionally useful for certain specimens and of little value in others. This has been the topic of countless investigations and "shoot-outs" at microscopy workshops and demonstrations. Needless to say, as with all techniques, there are some samples that are more appropriate than others (Murray, Appleton, Swedlow, & Waters, 2007). Deconvolution microscopy in general works in applications where the biological targets are small and where the density of labeling is relatively low. For example, deconvolution microscopy is ideally suited for studying cells and tissues in the range of 1–15 μm. Of course, there are some samples of tremendous depth (100 μm or so) where deconvolution has worked spectacularly, and there are some samples of shallow depth (<1 μm) that are impossible to image. Highly scattering and absorptive samples are extremely hard to optically image without mechanical sectioning.

One application where deconvolution often excels is in live-cell imaging up to a few cell layers deep. Live-cell imaging poses unique challenges to microscopy and especially fluorescence microscopy. Fluorescence is inherently an inefficient methodology. A tremendous number of excitation photons must be created in order to obtain even a modest number of emission photons. By some estimates, the most efficient microscopy systems yield approximately one detected photon for every 10^5 excitation photons (at the light source). As optical methods are deployed that eliminate emission photons (such as confocal) or that rely on rare nonlinear excitation (like multiphoton microscopy), the efficiencies decrease dramatically. Murray et al. estimate that spinning disk confocal microscopes are approximately 5% as efficient as wide-field systems and point-scanning confocal systems can be as little as 0.5% as efficient as wide-field systems. This often has tremendous implications for live-cell imaging. Many cells are poorly equipped for handling large photon doses. If one considers a cardiomyocytes in an intact human, that cell would rarely if ever be exposed to a photon with a wavelength of less than 1000 nm; consequently, it has few mechanisms for dealing with more energetic photons at shorter wavelengths. A wide-field microscope with a high-NA objective lens typically exposes a cell to roughly the same photon flux as sitting out in direct daylight. A point-scanning confocal may be 10,000 times higher, and a two-photon microscopy system can easily be 10,000 times higher than that. Some calculate the density of photons in a two-photon system to be higher than the photon density on the surface of the sun. Anything that can be done to reduce the photon flux on cells will help to minimize photodamage to the cell (Chapter 5).

Since we have established that deconvolving microscope images generally increases the contrast 10- to 100-fold, we can design experiments where this improvement is relied on. With deconvolution, we can often collect images with lower than desired contrast and count on the improvement that the algorithm affords. Lower contrast for the same hardware system translates into a combination of lower and shorter illumination onto the cell. This can lead to dramatic improvements in cell viability.

Deconvolution microscopy is not always effective. First of all, it is typically more effective with high-NA optics than it is with low-NA optics. Below an NA of 0.75, there is little axial resolution and contrast such that the algorithm has little information to work with. Very dense labeling can be problematic, again due to poor lateral and axial contrast. Samples that are highly scattering are difficult for all imaging systems, but the method of image formation in point-scanning systems can yield superior results over wide-field systems. Deconvolution microscopy works best with 3D data sets, while a confocal microscope system does not require 3D acquisition. This can yield faster results than deconvolution. This can be critical in attempting to image very rapidly moving objects, although new fast imaging modalities and brighter fluorescent probes (Chapter 6) mitigate much of this problem.

CONCLUSION

Deconvolution microscopy can be a highly effective method of enhancing the resolution and contrast of the optical microscope while enabling reduced photon load on the specimen. For many biological specimens, this improvement offers equivalent or better resolution than confocal or multiphoton systems while producing significant improvements in cell viability. Deconvolution can be linear and can maintain mass–intensity relationships in samples if properly deployed.

A general rule of thumb is to use only as much technology as the sample demands. If wide-field microscopy is sufficient, then there is no need for deconvolution. If deconvolution is necessary and sufficient, then there is no need for a confocal system. If the sample can tolerate higher photon flux and demands more contrast than deconvolution can deliver, then a confocal or even multiphoton system may be required.

As with all instrumentation, there is no single technology that can address all of the needs of a scientist; however, deconvolution has a proved history of being an important tool for microscopists and cell biologists.

REFERENCES

Agard, D. A. (1984). Optical sectioning microscopy: Cellular architecture in three dimensions. *Annual Review of Biophysics and Bioengineering*, *13*, 191–219.

Conchello, J. A. (1998). Superresolution and convergence properties of the expectation-maximization algorithm for maximum-likelihood deconvolution of incoherent images. *Journal of the Optical Society of America*, *15*, 2609–2619.

Frieden, B. R. (1975). Image enhancement and restoration. In T. S. Huang (Ed.), *Topics in applied physics: Picture processing and digital filtering: Vol. 6.* (pp. 177–248). New York, NY: Springer-Verlag.

Gold, R. (1964). *An iterative unfolding method for response matrices: Report No. ANL-6984*. Chicago, IL: Argonne National Laboratory.

Goodman, J. W. (2005). *Introduction to Fourier optics* (3rd ed.). Englewood, CO: Roberts and Company.

Goodwin, P. C. (2007). Evaluating optical aberrations using fluorescent microspheres: Methods, analysis, and corrective actions. In L. Wilson & P. Matsudura (Series Eds.) & G. Sluder & D. E. Wolf (Vol. Eds.), *Methods in cell biology: Vol. 81*. (pp. 397–413). London: Elsevier.

Hiraoka, Y., Sedat, J. W., & Agard, D. A. (1990). Determination of three-dimensional imaging properties of a light microscope system. Partial confocal behavior in epifluorescence microscopy. *Biophysical Journal*, *57*(2), 325–333.

Holmes, T. J. (1992). Blind deconvolution of quantum-limited imagery: Maximum-likelihood approach. *Journal of the Optical Society of America*, *9*, 1052–1061.

Jansson, P. A. (Ed.), (1997). *Deconvolution of images and spectra* (2nd ed.). New York, NY: Academic Press.

McNally, J. G., Karpova, J. G., Cooper, J., & Conchello, J. A. (1999). Three-dimensional imaging by deconvolution microscopy. *Microscopy Methods*, *19*, 373–385.

Mertz, J. (2010). *Introduction to optical microscopy*. Greenwood Village, CO: Roberts and Co.

Murray, J. M., Appleton, P. L., Swedlow, J. R., & Waters, J. C. (2007). Evaluating performance in three-dimensional fluorescence microscopy. *Journal of Microscopy*, *228*, 390–405.

Shaw, P. J. (1993). Computer reconstruction in three-dimensional fluorescence microscopy. In D. Shotton (Ed.), *Electronic light microscopy*. New York, NY: Wiley-Liss.

Shaw, P. J., & Rawlins, D. J. (1991). Three-dimensional fluorescence microscopy. *Progress in Biophysics and Molecular Biology*, *56*, 187–213.

Swedlow, J. R. (2007). Quantitative fluorescence microscopy and image deconvolution. In L. Wilson & P. Matsudura (Series Eds.) & G. Sluder & D. E. Wolf (Vol. Eds.), *Digital microscopy*. *Methods in cell biology: Vol. 81*. (pp. 447–465). London: Elsevier.

Swedlow, J. R., Hu, K., Andrews, P. D., Roos, D. S., & Murray, J. M. (2002). Measuring tubulin content in *Toxoplasma gondii*: A comparison of laser-scanning confocal and wide-field fluorescence microscopy. *Proceedings of the National Academy of Sciences of the United States of America*, *99*(4), 2014–2019.

Swedlow, J. R., Sedat, J. W., & Agard, D. A. (1997). Deconvolution in optical microscopy. In P. A. Jansson (Ed.), *Deconvolution of images and spectra* (2nd ed.). New York, NY: Academic Press.

Wallace, W., Schaefer, L. H., & Swedlow, J. R. (2001). A workingperson's guide to deconvolution in light microscopy. *BioTechniques*, *31*, 1076–1097.

White, N. S., Errington, R. J., Fricker, M. D., & Wood, J. L. (1995). Aberration control in quantitative imaging of botanical specimens by multidimensional fluorescence microscopy. *Journal of Microscopy*, *181*(2), 99–116.